Inositol triphosphate-triggered calcium release blocks lipid exchange at endoplasmic reticulum-Golgi contact sites

Charles Malek
Leibniz-Forschungsinstitut für Molekulare Pharmakologie https://orcid.org/0000-0002-7523-7593
Anna Maria Wawrzyniak
KULeuven
Peter Koch
Leibniz-Forschungsinstitut für Molekulare Pharmakologie
Christian Lüchtenborg
Biochemie-Zentrum Uni HD
Manuel Hessenberger
Leibniz-Leibniz-Forschungsinstitut für Molekulare Pharmakologiefür Molekulare Pharmakologie
Timo Sachsenheimer
Heidelberg University
Wonyul Jang
Leibniz-Forschungsinstitut für Molekulare Pharmakologie
Britta Bruegger
Ruprecht-Karls-Universität Heidelberg
Volker Haucke (haucke@fmp-berlin.de)
Leibniz-Forschungsinstitut für Molekulare Pharmakologie https://orcid.org/0000-0003-3119-6993

Article

Keywords: calcium, cholesterol export repression, lipid exchange, endoplasmic reticulum-Golgi contact sites

Posted Date: July 16th, 2020

DOI: https://doi.org/10.21203/rs.3.rs-35925/v1

Version of Record: A version of this preprint was published at Nature Communications on May 11th, 2021. See the published version at https://doi.org/10.1038/s41467-021-22882-x.

Abstract

Vesicular traffic and membrane contact sites between organelles enable the exchange of proteins, lipids, and metabolites. Recruitment of membrane tethers to contact sites between the endoplasmic reticulum (ER) and the plasma membrane is often triggered by calcium. In contrast, we reveal here a function for calcium in the repression of cholesterol export at membrane contact sites between the ER and the Golgi complex. We show that calcium efflux from ER stores induced by inositol-triphosphate [IP3] accumulation upon loss of the inositol 5-phosphatase INPP5A or sustained receptor signaling triggers the depletion of cholesterol and associated complex glycosphingolipids from the cell surface, resulting in a blockade of clathrin-independent endocytosis (CIE) of bacterial toxins. This phenotype is caused by the calcium-induced dissociation of oxysterol binding protein (OSBP) from the Golgi complex and from VAP-containing membrane contact sites. Our findings reveal a crucial function for INPP5A-mediated IP3 hydrolysis in the control of lipid exchange at membrane contact sites.

Introduction

Cellular membrane homeostasis and the exchange of material between compartments can occur by vesicular traffic along the endocytic and secretory pathways [1, 2], and by membrane contact sites (MCS), i.e. areas where organelles are in close apposition [3, 4, 5, 6, 7]. For example, the endoplasmic reticulum (ER) has been found to form MCS with essentially all other organelles including the plasma membrane, mitochondria, endosomes, lysosomes, and the trans-Golgi network (TGN) to facilitate calcium homeostasis and signaling [8, 9] and the exchange of lipids [5, 7, 10]. A major physiological role of MCS is non-vesicular lipid exchange by lipid-transport proteins such as the members of the oxysterol binding protein (OSBP) family. The founding member OSBP has been shown to exchange cholesterol, a major constitutent of the plasma membrane, and phosphatidylinositol 4-phosphate [PI(4)P], a lipid enriched in the Golgi complex, at MCS between the ER and the TGN formed by ER-localized VAP-A/B proteins that act as membrane tethers [11, 12, 13]. Inhibition of OSBP function causes the re-routing of cholesterol to ER-derived lipid droplets and the concomitant depletion of cholesterol from the Golgi complex and, partially, from the plasma membrane [11].

Cholesterol tightly associates with glycosphingolipids and proteins in cell membranes [14, 15]. Hence, loss of cholesterol is expected to affect a multitude of cellular functions [16, 17, 18, 19, 20]. These range from the formation of glycosphingolipid-dependent signaling and trafficking platforms [17, 18, 21] to the clathrin-independent endocytosis (CIE) of cell adhesion molecules [22] and bacterial toxins, e.g. Shiga toxin[23, 24, 25]. Cellular uptake of Shiga toxin is initiated by binding to the cholesterol-associated [25] complex glycosphingolipid globotriosylceramide (Gb3) followed by cholesterol-dependent membrane reorganization [24] that results in the formation and fission of endocytic membrane vesicles[26]. Similar pathways of CIE control the surface levels and activity of cell signaling receptors [27, 28], including receptors (e.g. G protein-coupled receptors) linked to phospholipase C (PLC). This enzyme hydrolyzes plasma membrane phosphatidylinositol 4,5-bisphosphate [$PI(4,5)P_2$] to generate the soluble messenger

inositol 1,4,5-triphosphate (IP_3), which triggers an increase in cytoplasmic calcium levels [29, 30] that, in turn, may affect MCS [5, 8]. These findings suggest a close, albeit poorly understood, interplay between non-vesicular lipid transport via membrane contact sites, calcium signaling, and the cholesterol- and glycosphingolipid-dependent formation of endocytic vesicles during CIE.

To address this interplay we conducted a screen using a focussed siRNA library targeting human phosphoinositol kinases and phosphatases for regulators of cell entry of bacterial Shiga toxin. We identified the inositol phosphatase INPP5A. INPP5A is a ubiquitously expressed plasma membrane-associated [31] inositol 5-phosphatase that specifically hydrolyzes IP_3 (and IP_4) to repress calcium signaling [32] and is downregulated in cancer and spinocerebellar ataxia type 17 [33, 34, 35, 36, 37]. We found that IP_3-triggered calcium efflux from the ER in the absence of INPP5A blocks Shiga toxin endocytosis as a result of impaired cholesterol transport to the Golgi complex and the concomitant depletion of cholesterol-associated complex glycosphingolipids such as Gb3 from the plasma membrane. We further demonstrate that this phenotype is a consequence of the calcium-induced dissociation of OSBP from the TGN and from VAP-containing MCS. The inhibitory role of calcium with respect to OSBP/ VAP-mediated MCS formation is, thus, distinct from the established function of calcium in facilitating STIM1-ORAI channel formation [9, 29] and the recruitment of ER-localized E-Syts to ER-plasma membrane contact sites [5, 7, 38].

These results have important implications for our understanding of the interplay between calcium signaling and cellular lipid homeostasis and bear implications for diseases such as cancer and ataxia associated with altered INPP5A levels or function.

Results

INPP5A is required for glycosphingolipid-mediated cell entry of bacterial toxins

Given the pivotal roles of inositol lipids in the regulation of membrane traffic [1, 39] we screened an siRNA smart pool library encoding all known human inositol kinases and phosphatases for a possible function in the internalization of Shiga toxin, a bacterial toxin known to enter cells via a glycosphingolipid-mediated clathrin-independent endocytosis (CIE) pathway. Consistent with the established function of phosphatidylinositol-bisphosphates in endocytosis[1, 27, 40], we found CIE of Shiga toxin to be strongly reduced upon cellular depletion of phosphatidylinositol (PI) 4-phosphate 5-kinase type IB (PIPKIB) or PI 3-kinase C2γ(PI3KC2G), i.e. enzymes that synthesize plasma membrane $PI(4,5)P_2$ or phosphatidylinositol (3,4)-bisphosphate [$PI(3,4)P_2$] [40, 41], respectively (Figure 1a). Our attention, however, was caught by the adverse effects of knockdown of the inositol 5-phosphatase INPP5A, an enzyme known to predominantly hydrolyze non-membrane bound soluble inositol phosphates such as inositol 1,4,5-triphosphate [IP_3] [34,

[36, 42], the product of $PI(4,5)P_2$ cleavage by phospholipase C downstream of receptor signaling [32]. Hence, we explored the molecular pathway and mechanism underlying the putative role of INPP5A in CIE.

Shiga toxin endocytosis is known to be initiated by the tight association of its oligomeric B subunit with Gb3 glycosphingolipids on the cell surface [25, 26, 28]. Defective CIE of Shiga toxin in INPP5A-depleted cells therefore could either reflect a requirement for INPP5A in the internalization step of CIE or in the regulation of Gb3 levels at the cell surface. Impaired CIE of Shiga toxin upon effective knockdown of INPP5A (Figure 1b) was paralleled by a proportional decrease in binding of Shiga toxin to the surface of INPP5A-depleted HeLa cells (Figure 1c,d), suggesting that Gb3 is depleted from the plasma membrane of cells lacking INPP5A. A requirement for INPP5A in the Gb3-dependent uptake of Shiga toxin was further confirmed in INPP5A knockout HAP1 cells generated by CRISPR/ Cas9 (Figure S1a). In contrast, CME of transferrin or internalization of EGF proceeded unperturbed in INPP5A-depleted cells (Figures 1e, S1c). No alterations in the amounts of transferrin or EGF receptors at the plasma membrane or in the levels of surface glycoproteins detected by wheat germ agglutinin were detected upon loss of INPP5A (Figure S1d,e). INPP5A depletion, thus, appears to impair CIE of bacterial toxins by reducing the surface levels of complex glycosphingolipids including Gb3. We challenged this hypothesis by analyzing the endocytic uptake of Cholera toxin, a complex glycosphingolipid-binding bacterial toxin internalized in part by CIE [28, 43]. Endocytosis of Cholera toxin was reduced by more than 50% in INPP5A-depleted cells (Figure 1f, S1b, f). Importantly, exogenous supplementation of INPP5A-depleted cells with high concentrations of GM1, the cellular glycosphingolipid receptor for Cholera toxin [43], rescued defective Cholera toxin endocytosis (Figures 1f, S1f). These data indicate that INPP5A controls the cell surface levels of complex glycosphingolipids including Gb3 and GM1, and thereby, CIE of bacterial toxins.

Loss of Gb3 is caused by impaired OSBP-mediated cholesterol export in absence of INNP5A

Reduced cell surface levels of complex glycosphingolipids such as Gb3 and GM1 in INPP5A-depleted cells could arise either from (i) defects in lipid biosynthesis, or (ii) be caused indirectly as a consequence of impaired lipid transport, e.g. by defective transport of complex glycosphingolipids from the Golgi complex, i.e. their site of synthesis, to the plasma membrane. To examine whether INPP5A loss impacts on total cellular lipid composition, we quantitatively analyzed lipids from total extracts of control- and INPP5A-depleted HeLa cells by nano-electrospray ionization tandem mass spectrometry as described [44, 45]. No alterations were detected in the amounts or relative fractions of glycerophospholipids (e.g. e.g. phosphatidylcholine, phosphatidylethanolamine, phosphatidylserine, phosphatidic acid, phosphatidylinositol, phosphatidylglycerol) and neutral lipids (diacylglycerol and triacylglycerol). (Table S1). The total cellular amounts of cholesterol or sphingomyelin were also unaltered (Figure 2a). We also failed to detect any changes in the amounts of ceramide, the main substrate for sphingolipid synthesis, in the levels of simple glycosphingolipids such as monohexosylceramides or di-hexosylceramides (e.g. lactosylceramide) (Figure 2b). Unaltered levels and distribution of ceramide, the common precursor for all

glycosphingolipids [46] was confirmed by confocal image analysis of HeLaM cells stained with antibodies against ceramide (Figure 2c). The total content of the complex glycosphingolipids GM3 and GM1 was moderately increased, while that of tri-hexosylceramides including Gb3 was marginally decreased (to about 77% of controls) in INPP5A-depleted cells (Figure 2d). Hence, loss of INPP5A does not alter the total cellular phosphoglycerolipid to glycosphingolipid ratio and leads to minor changes in complex glycosphingolipid composition (Figure 2, Table S1). These results make it unlikely that INPP5A loss inhibits CIE of bacterial toxins by blocking lipid biosynthesis.

We therefore followed the alternative hypothesis that the depletion of Gb3 and GM1 from the cell surface might reflect defects in their transport to the plasma membrane. Earlier work had revealed a close physical association of complex glycosphingolipids including Gb3 and GM1 with cholesterol including the formation of microdomains at the levels of the Golgi complex [47] and the plasma membrane [17, 18, 21, 25, 48]. We therefore hypothesized that the reduced surface levels of complex glycosphingolipids such as Gb3 might be a consequence of defective cholesterol export from the ER in the absence of INNP5A.

Visualization of the overall distribution of cholesterol by Filipin suggested that cholesterol is partially redistribruted from the cell surface to intracellular organelles in INPP5A-depleted cells (Figure 3a). Moreover, specific labeling of plasma membrane cholesterol with the recombinant purified GFP-tagged domain 4 (D4) of Perfringolysin O (PFO, theta toxin), a cholesterol-binding toxin [49], revealed reduced cholesterol levels in the exoplasmic plasma membrane leaflet of INPP5A-depleted cells compared to SCR siRNA-treated controls (Figure 3b,c). The apparent reduction in plasma membrane cholesterol in INPP5A-depleted cells was paralleled by a corresponding prominent increase of intracellular cholesterol puncta detected by cytosolic expression of DH4-mCherry (Figure 3d) and BODIPY (493/503) labeling to visualize cholesterol-enriched lipid droplets (Figure 3e,f). Consistent with a key role for cholesterol in stabilizing Gb3 glycosphingolipids in the Golgi complex and at the cell surface, we found surface binding (Figure 3g, S2g) and internalization (Figure 3h, S2a) of Shiga toxin to be severely compromised in HeLa cells treated with Mevastatin to block cholesterol biosynthesis. These data suggest that in the absence of INPP5A cholesterol fails to be transported from the ER to the Golgi complex and, instead, is sorted to ER-derived lipid droplets.

The transport of newly synthesized cholesterol from the ER, its site of synthesis, to the Golgi complex requires its oxysterol-binding protein (OSBP)-mediated transfer via VAP-containing membrane contact sites [11]. In this mechanism OSBP exchanges cholesterol present in ER membranes with phosphatidylinositol 4-phosphate [PI(4)P], a lipid highly enriched at the Golgi complex and the TGN [50]. As a result cholesterol is transferred from the ER to the TGN, while PI(4)P is transported retrogradely to the ER, where its phosphate is hydrolyzed by SAC1, thereby powering the OSBP cycle [11, 50, 51]. Loss of OSBP function has been shown to cause the accumulation of cholesterol at the ER and in lipid droplets and a concomitant rise in PI(4)P levels at the Golgi complex [11]. As loss of INPP5A also led to a redistribution of cholesterol to ER-derived lipid droplets akin to inhibition of OSBP function (Figure 3e,f), we probed whether this defect was accompanied by accumulation of PI(4)P in the Golgi compartment/ TGN. Indeed,

we observed profoundly elevated levels of Golgi/ TGN-localized PI(4)P and a compaction of the TGN in INPP5A-depleted cells (Figure 4a-d). In contrast, no elevation in the level of $PI(4,5)P_2$, a lipid predominantly localized to the plasma membrane and a potential substrate of INPP5A was observed (Figure S2b,c) (consistent with [42]). Moreover, cellular depletion of OSBP (Figures 4e, S2d,e), pharmacological inhibition of OSBP-mediated cholesterol/ PI(4)P exchange in the presence of the OSBP-specific small molecule inhibitor OSW–1 [11] (Figures 4f,g S2f,g), or CRISPR/ Cas9-mediated knockout of the OSBP binding partner VAP-A/B [52](Figure 4h, S2e) phenocopied loss of INPP5A with respect to defective surface binding and CIE of Shiga toxin.

Collectively, these results indicate that the reduced plasma membrane levels of complex glycosphingolipids (e.g. Gb3) in INPP5A-depleted cells are a consequence of impaired OSBP-mediated cholesterol/ PI(4)P exchange at ER/ Golgi membrane contact sites. They further suggest that OSBP-mediated cholesterol export from the ER to the Golgi complex at MCS is required for glycosphingolipid transport from the Golgi complex to the plasma membrane, a process regulated by INPP5A.

IP_3-induced calcium release downstream of receptor activation represses glycosphingolipid-dependent toxin CIE

Next we aimed to unravel the pathway by which loss of INPP5A represses OSBP-mediated cholesterol export and, thereby, inhibit the glycosphingolipid-dependent CIE of bacterial toxins. INPP5A has been been demonstrated to predominatly hydrolyze soluble IP_3 [34, 42] and, thus, may constitute a negative regulatory element in the signaling cascade that triggers IP_3 receptor (IP_3R)-mediated calcium release from the ER lumen via PLC-mediated cleavage of $PI(4,5)P_2$ into diacylglycerol and IP_3 downstream of receptor activation (Figure 5a). We therefore hypothesized that elevated IP_3 levels in absence of INPP5A might repress OSBP function, and, thereby, Shiga toxin CIE. We tested the putative role of IP_3 in this pathway at multiple levels using CIE of Shiga toxin as a functional readout. First, we analyzed the cellular content of IP_3. As expected, the levels of IP_3 were increased about two-fold in INPP5A-depleted cells (Figure 5b). Second, we reasoned that, if elevated IP_3 levels were causative for defective Gb3-dependent Shiga toxin entry into INPP5A knockdown cells, other independent manipulations of IP_3 turnover should phenocopy loss of INPP5A. IP_3 can either be hydrolyzed to IP_2 by inositol 5-phosphatases, most notably INPP5A, or be further phosphorylated by inositol triphosphate kinase B (ITPKB) to yield IP_4 [53, 54]. We found that cellular depletion of ITPK reduced surface binding and internalization of Shiga toxin (Figures 5c, S3a) or Cholera toxin (Figures 5d, S3b), akin to INPP5A loss. Co-depletion of both INPP5A and ITPK resulted in synergistic effects, i.e. a near complete blockade of Shiga toxin binding and CIE (Figures 5c, S3a). To acutely elevate IP_3 levels, we applied PEI-II, a blocker of prolyl oligopeptidase that indirectly stimulates IP_6-to-IP_3 conversion via multiple inositol phosphate phosphatase (MIPP) [55]. Application of PEI-II for 16 hours also significantly reduced Shiga toxin CIE in genetically unperturbed wild-type HeLa cells (Figures 5e, S3c). Third, we probed whether the IP_3-phosphatase activity of INPP5A is required for

Shiga toxin endocytosis. Defective CIE of Shiga toxin was fully rescued by re-expression of active wild-type but not phosphatase-deficient INPP5A (Figures 5f, S3d,e). The impaired glycosphingolipid-dependent Shiga toxin CIE in the absence of INPP5A, thus, appears to be caused by elevated IP3 levels.

IP_3 mainly acts by activating IP_3 receptor (IP_3R) channels in the ER to release calciuminto the cytoplasm. Consistent with this, we found INPP5A-depleted cells to display increased cytosolic calcium levels monitored by Fluo4 (Figure 5g,h). To probe whether elevated calcium levels were causal for the blockade of Shiga toxin CIE in absence of INPP5A, we perturbed IP_3-induced calcium efflux from the ER by depleting HeLa cells of IP_3Rs. Knockdown of IP_3R expression by smart pool siRNAs indeed partially rescued impaired Shiga toxin endocytosis in INPP5A-depleted cells (Figures 5i, S3f). Finally, we perturbed the activation status of PLC, i.e. the enzyme that generates IP_3 downstream of receptor signaling. Pharmacological activation of PLC by m–3M3FBS potently repressed CIE of Shiga toxin (Fig. 5j, S4a). Conversely, impaired Shiga toxin uptake in INPP5A-depleted cells was largely rescued by PLC inhibition in the presence of D609 (Fig. S4b,c). Hence, INPP5A controls glycosphingolipid-dependent CIE of bacterial toxins by hydrolyzing IP_3, thereby counteracting IP_3-induced calcium efflux via IP_3Rs from ER stores downstream of signaling receptor activation.

Calcium triggers OSBP dissociation from Golgi membranes and from VAP-containing MCS

These results suggest a model according to which the cytosolic concentrations of IP_3 and/ or calcium regulate OSBP-mediated cholesterol export at ER/ Golgi MCS to control surface glycosphingolipid levels and, thereby, CIE of bacterial toxins. Given that OSBP-mediated lipid exchange requires the association of Golgi-localized OSBP with VAP proteins in the ER [13, 50], we hypothesized that INPP5A by controlling IP_3 levels might impact on complex formation between VAP and OSBP proteins. Complex formation between OSBP-GFP and VAP-A-HA probed by co-immunoprecipitation experiments indeed was reduced by nearly 50% in INPP5A-knockdown cells. Importantly, a similar effect was observed in control HEK293-T cells, in which IP_3 levels were acutely raised by application of cell membrane-permeant IP_3/AM (Figure 6a,b).

VAP is a transmembrane protein of the ER, whereas OSBP associates with the TGN via binding of its pleckstrin homology (PH) domain to PI(4)P [50, 51]. Hence, we speculated that the accumulation of IP_3 in the absence of INPP5A either directly or indirectly via IP_3-induced calcium efflux from the ER might interfere with the recruitment and localization of OSBP to the TGN. Confocal imaging showed that while endogenous OSBP was concentrated in the TGN/ Golgi area in close apposition to the Golgi marker GM130 in control cells, it adopted a largely dispersed localization in the cytoplasm of INPP5A-depleted cells (Figure 6c,d,). A similar, though even more striking loss of OSBP from TGN/ Golgi membranes was observed in HeLa cells treated with cell membrane-permeant IP_3/AM (Figure 6e,f), indicating that IP_3 and/ or calcium released from ER stores negatively regulate the association of OSBP with the TGN in living cells. Conceivably, the negative regulatory role of IP_3 with respect to OSBP recruitment to the TGN could

reflect competition of IP_3 with PI(4)P via its charged phosphate-rich inositol headgroup or be mediated indirectly via elevated calcium levels in the cytosol that may shield the headgroup of PI(4)P from recognition by the PH domain of OSBP [56]. To distinguish between these mechanisms, we assayed the recruitment of purified recombinant OSBP-PH domain to PI(4)P-containing liposomes *in vitro.* Increasing concentrations of IP_3 up to 700 µM, i.e. well above physiological IP_3 levels, did not affect OSBP-PH binding to PI(4)P membranes (Figure 6g), consistent with a role for IP_3R-mediated calcium release from the ER lumen in the regulation of Shiga toxin CIE (compare Figure 5). In contrast, OSBP-PH binding to PI(4)P-containing liposomes was potently inhibited by micromolar calcium concentrations (Figure 6h,i), indicating that calcium directly interferes with the association of OSBP with PI(4)P-containing membranes (consistent with [57]) and, thereby, with its binding to VAP to promote lipid exchange. The association of the PH domain of the ceramide/ PI(4)P lipid exchange protein CERT with PI(4)P-liposomes was much less affected by increasing calcium concentrations (Figure 6h,i), in agreement with the unaltered levels and distribution of ceramide (Figure 2) in INPP5A knockdown cells.

Collectively, these results demonstrate that IP_3-triggered calcium release blocks lipid exchange mediated by OSBP at ER-Golgi contact sites to regulate cholesterol and associated complex glycosphingolipid surface levels (Figure 6j, model).

Discussion

Our results reported here reveal a hitherto unknown function for IP_3-triggered calcium release from the ER in the repression of cholesterol export at MCS between the ER and the TGN, a process controlled by the IP_3-specific-phosphatase INPP5A (Figures 3 and 4), an enzyme downregulated in cancer [34], e.g. squamous cell carcinomas [33], and spinocerebellar ataxia [37, 58]. Defective cholesterol export at ER/ TGN MCS is further demonstrated to reduce the plasma membrane levels but not the total cellular content of complex glycosphingolipids such as Gb3 and GM1 (Figure 1 and 2), likely as a consequence of their impaired assembly into transport-competent cholesterol-rich microdomains at the level of the Golgi complex [47], resulting in a blockade of CIE of bacterial toxins (Figures 1,3–5). Finally, elevated cytosolic calcium levels induced by IP_3-induced calcium release from ER stores in INPP5A-depleted cells are shown to inhibit membrane recruitment and localization of OSBP to the TGN via PI(4)P (Figure 6).

This hypothetical pathway is supported by multiple lines of evidence: (i) Loss of INPP5A is shown to cause the selective accumulation of IP_3 (Figure 5) but not of its precursor and potential substrate $PI(4,5)P_2$ from which it is derived (Figure S2a,b). The concomitant built-up of PI(4)P at the Golgi/ TGN (Figure 4) is explained by the observed mislocalization and loss-of-function of OSBP in INPP5A-depleted cells (Figure 6). Consistent with this model, (ii) we observe that impaired CIE of Shiga toxin is rescued by WT but not phosphatase-inactive INPP5A that lacks the ability to hydrolyze IP_3 or by co-depletion of IP_3 receptors (Figure 5), i.e. a condition that prevents IP_3-mediated calcium efflux from the ER lumen. Furthermore, (iii) we show that exogenous application of membrane-permeant IP_3 phenocopies loss of

INPP5A with respect to impaired CIE of Shiga toxin and depletion of OSBP from the TGN and from VAP-containing complexes (Figure 6), suggesting that the accumulation of IP_3 is not only required but also sufficient to induce the cellular phenotypes characteristic of INPP5A loss. Fourth, (iv) we use quantitative lipidomic analyses by mass spectrometry (Figure 2) to demonstrate that depletion of INPP5A does not alter total cellular lipid content including complex glycosphingolipids (i.e. receptor lipids for bacterial toxins such as Shiga toxin). Instead, complex glycosphingolipid loss from the surface of INPP5A-depleted cells is shown to be an indirect consenquence of defects in cholesterol export from the ER to the Golgi complex, which instead is rerouted to lipid droplets (Figure 3), a lipid storage compartment that buds from within the ER membrane. The key role of cholesterol in the maintenance of complex glycosphingolipids is further supported by the fact that acute blockade of cholesterol biosynthesis by Mevastatin (Figure 3), genetic or pharmacological inhibition of OSBP-mediated cholesterol transport out of the ER (Figure 4), or loss of ER/ TGN MCS in VAP-A/B KO cells (Figure 4) phenocopy INPP5A depletion with respect to loss of complex glycosphingolipids from the plasma membrane and defective CIE of Shiga toxin. Finally, (v) we demonstrate using purified components that low micromolar concentrations of calcium directly interfere with the association of the PH domain of OSBP with PI(4)P-containing membranes, whereas membrane association of other PI(4)P-binding PH domains such as that of CERT is less affected (Figure 6). These latter data are consistent with and explain the impairment of cholesterol export to the TGN/ Golgi complex and to the cell surface, In contrast, transport of ceramide via CERT to produce sphingomyelin appears to proceed unaltered (Figure 2, Table S1). Finally, we observed only minor effects of INPP5A depletion on the localization of the PI(4)P-binding glucosylceramide transfer protein FAPP2 [59] at the TGN (Figure S5).

At the moment we can only speculate about the exact mechanism by which impaired cholesterol export from the ER to the TGN under conditions of INPP5A or VAP loss causes the depletion of complex glycosphingolipids such as Gb3 and GM1 from the cell surface. We note that previous studies have established a tight physical and functional connection between cholesterol and complex glycosphingolipids such as Gb3 and GM1, e.g. as constituents of microdomains in the Golgi complex [47], as GPI-linked signalling complexes, or as key regulators of endocytic tubule formation that mediate cell entry of bacterial toxins including Shiga toxin [17, 18, 23, 24, 25, 28]. Acute cholesterol depletion has been demonstrated before to perturb the transport of complex glycosphingolipids such as GM1 [60] akin to our results reported here. We, thus, hypothesize that defective cholesterol export to the TGN affects complex glycosphingolipids at the level of the Golgi complex, where they are synthesized. For example, it is possible that under conditions of impaired cholesterol export from the ER in INPP5A-, OSBP-, or VAP-depleted cells complex glycosphingolipids following their biosynthesis fail to assemble into stable microdomains in the late Golgi [47] and, therefore, fail to be transported to the plasma membrane. Future studies will be needed to explore this mechanism in more detail.

Our findings also expand previous studies on the regulation of MCS by calcium signalling [5, 7, 8]. Distinct from the established function of cytoplasmic calcium signals in triggering STIM1-ORAI channel formation [9, 29] and the recruitment of ER-localized E-Syts to ER-plasma membrane contact sites, we

observe an inhibitory role of calcium with respect to OSBP/ VAP-mediated lipid exchange at ER-TGN contacts. E-Syts are ER-localized C2 domain proteins that bind to the plasma membrane in trans via recognition of $PI(4,5)P_2$ by their so-called C2 domains. In the case of E-Syt1 micromolar concentrations of calcium, e.g. induced by receptor signaling via PLC-triggered IP_3-induced calcium release from ER stores [38], promote its association with the plasma membrane to transfer glycerolipids such as diacylglycerol [4, 5], between the plasma membrane and the ER. We now show that a similar pathway via IP_3-induced calcium release from the ER (Figure 5) represses the exchange of cholesterol and PI(4)P at ER/ TGN contact sites by calcium-mediated inhibition of OSBP recruitment to PI(4)P-containing TGN membranes. It therefore appears that signaling via PLC-coupled receptors differentially affects lipid exchange via E-Syts at ER/ plasma membrane *vs.* OSBP at ER/ TGN contact sites. It is conceivable that the physiological effects of IP_3-induced calcium release from the ER [8, 29] may also affect non-vesicular lipid transport at other intracellular MCS that depend on phosphosphoinositide-based membrane tethers, for example ER-endosome [52, 61] or ER-lysosome contacts [3, 4, 6]. Given that several types of MCS play key roles in calcium channeling and homeostasis [8] it is tempting to speculate that MCS formation and function may be part of a feedback-regulated molecular network that serves to integrate lipid flux with signalling-induced fluctuations in calcium levels [8, 29]. Whether and how this network impinges on the IP_3-phosphatase INPP5A itself, is unclear. Previous work had suggested that INPP5A may be regulated by phosphorylation-dependent association with inhibitory 14–3–3 proteins [62]. Our attempts to determine the precise localization and mode of regulation of endogenous INPP5A have been unsuccessful so far, largely owed to its low levels of expression.

We further show that loss of INPP5A and the resulting depletion of plasma membrane cholesterol and associated complex glycosphingolipids from the cell surface potently blocks CIE of bacterial toxins. Glycosphingolipids also play important roles in other forms of CIE such as the internalization of CD44 and integrins via the CLIC/GEEC pathway [22], which may conceivably be regulated by IP_3 signaling and turnover mediated by INPP5A. CIE pathways similar to the Shiga toxin route of entry control the surface levels and activity of PLC-linked cell signalling receptors [26, 27, 28, 63]. In this context it is interesting to note that reduced expression of INPP5A and changes in the synthesis and/ or surface expression of glycosphingolipids and cholesterol have been associated with cancer and metastasis [16, 20], processes regulated by the exo-endocytosis of cell signalling and adhesion receptors such as integrins, and with regulated cell death by apoptosis [64]. Reduced expression of INPP5A has also been found to be involved in spinocerebellar ataxia [37, 58], a group of neurodegenerative diseases that includes forms intimately linked to defective Golgi-to-plasma membrane trafficking [65, 66]. Exploring these mechanisms in detail remains a fruitful area for future studies.

Methods

siRNAs. siRNA oligonucleotides used in this study (SMART pools consisting of 4 siRNAs) are listed in Supplementary Table 1.

Antibodies. Antibodies used in this study are listed in Supplementary Table 2.

Antibodies used for immunoblotting and immunocytochemistry. Secondary antibodies for immunoblotting were either Peroxidase-conjugated for horse radish peroxidase (HRP)-detection or conjugated to a fluorescent dye for fluorescence detection. Secondary antibodies for immunocytochemistry were Alexa Fluor (AF)-conjugated. ICC—immunocytochemistry; IB—immunoblotting; rb - rabbit, ms—mouse, r—rat, gt—goat; dk - donkey; AF –Alexa Fluor; α—anti; H & L—heavy and light chain.

Plasmids.

pcDNA3.1(+),EcoRV/XbaI-INPP5Awt, pcDNA3.1(+),EcoRV/XbaI-INPP5Apase dead, were designed with GeneArt services from ThermoFisher. D4Hmcherry-pGEX–6P1 is a gift from Pr. Gregory D Fairn. pEGFP-N1-OSBP is a gift from Pr. Pietro De Camilli and pGW-VAP-HA was a gift from Pr. Caspar C. Hoogenraad

Chemicals and inhibitors. All Chemicals and inhibitors were dissolved according to the manufacturer instructions to indicated concentrations at stock solutions. Working concentrations are indicated for each experiment. OSW–1 targeting OSBP was prepared in a stock solution of 2 µM and purchased from BOC Sciences (B0005–092456). Bt3-Ins(145)P3/AM was prepared at 100 mM stock solution and purchased from Sichem (3–1–145). PEI-II was prepared at 24mM stock solution and purchased from Sigma-Aldrich (537011). MevastatinSodium was prepared at 30mg/ml stock solution and purchased from Sigma-Aldrich (474705), GM1 was purchased from Sigma-Aldrich (G7641). D609 was prepared at 10mM stock solution and purchased from TOCRIS (1437). m–3M3FBS was prepared at 10mM stock solution and purchased from Sigma-Aldrich (525185).

Probes. We purschased from Sigma-Aldrich; Shiga Toxin Subunit B (SML0562) and prepared a stock solution of 100µg/ml. Cholera Toxin Subunit B (C9903-.5MG) and prepared at 1mg/ml. Filipin III (F4767) and prepared it at 25 mg/ml. We purschased from Thermo-Fisher; BODIPY (D3922) and prepared it at 2mM. EGF-Alexa Fluor 647 (E35351) and prepared it at 40 µg/mL. Tf-Alexa Fluor 647 (T23366) and prepared it at 5mg/ml. WGA Alexa Fluor 647 (W32466) and prepared it at 1mg/ml. Fluo–4 (F14201) and prepared it at 1 mM.

Cells. HeLa and HEK293T and COS7 cells were obtained from the American Type Culture Collection. Cells were cultured in DMEM with 4.5 g l−1 glucose (Lonza) containing 10% heat-inactivated FBS (Gibco) and 100 U ml−1 penicillin and 100 µg ml−1 streptomycin (Gibco) during experimental procedures. Human INPP5A 4bp deletion knockout cell line and C631 Human HAP1 parental control cell line were purchased from Horizon Discovery. VAP_A/B Double knocked-out and parental HeLa cells were a gift from Pr. Pietro De Camilli's laboratory. Cells were routinely tested for Mycoplasma contamination and all tests were negative.

siRNA, cDNA transfections. 100,000 (Hela, HeLaM, COS–7) cells or 300,000 HEK293T cells, with low passage numbers, are reverse-transfected using jetPRIME transfection reagent according to the

manufacturer protocol using 100 nM of each siRNA. If DNA cotransfection is needed, cells are first reverse-transfected with siRNA, and 24 hours later, 2 ug of DNA is transfected using the jetPRIME protocol.

Inositol–1,4,5-Trisphosphate measurement. IP3 was determined using the Inositol–1,4,5-Trisphosphate [3H] Radioreceptor Assay Kit purchased from perkinelmer (NEK064). Briefly, 500,000 HeLa cells were treated with negative siRNA or siRNA against INPP5A for 48 hours, then cells were washed with PBS and trypsinized and collected into 500 ul of fresh medium then placed on ice. Immediately 100 ul of ice cold 100% TCA solution and vortexed thoroughly and Incubated in ice for 15 minutes. Centrifuged for 10 minutes 4° C at 1000 x g then we removed supernatant and discarded the pellet. We incubated supernatant solution for 15 minutes at room temperature, then we proceeded with the removal of Trichloroacetic Acid from Extracts and we measured the IP3 level in the samples using the principle of a membrane preparation derived from calf cerebellum which contains the IP3 receptor. This receptor binds natural inositol trisphosphate (IP3) and radiolabeled, tritiated inositol trisphosphate ([3H]IP3) The amount of [3H]IP3 bound to the receptor is measured by centrifuging the membranes into a pellet at the bottom of a centrifuge tube and counting the amount of radioactivity in the pellet.

PH domain expression and purification. The PH-domain of OSBP (87–190) and of CERT (24–117) were cloned into a Pet28a(+) Vector and expressed in *Escherichia coli* BL21 DE3 cells. Bacteria were cultured in 2xYT medium at 37 °C to an OD_{600} of 0.6 followed by a temperature shift to 18 °C. Protein was expressed for 18 h by adding 200 µM isopropyl β-D–1-thiogalactopyranoside. Cells were harvested by centrifugation, resuspended in lysis buffer containing 50 mM HEPES pH 7.5, 500 mM NaCl, 2mM DTT, 1 µM DNase (Roche) and 100 µM Pefabloc (Roth), and lysed by sonication. Lysates were cleared by centrifugation at 40,000*g* for 20 min at 4 °C. The supernatant was applied to a 1 ml Ni-NTA column pre-equilibrated with 50 mM HEPES/NaOH pH 7.5, 500 mM NaCl, 20 mM imidazole, 2mM DTT. The column was extensively washed with this buffer. His_6-tagged protein was eluted with 50 mM HEPES/NaOH pH 7.5, 500 mM NaCl, 300 mM imidazole, 2mM DTT and dialyzed against 50 mM HEPES/NaOH pH 7.5, 150 mM NaCl, 5mM DTT overnight at 4 °C. The protein was concentrated and flash frozen in liquid nitrogen.

Liposome co-sedimentation assay. Liposomes were produced by mixing PC:PE:SM:Chol:PI(4)P (Sigma and Avanti Lipids) in a molar ratio of 40:15:10:8:8, followed by drying under Argon stream and solubilization in 20 mM HEPES/NaOH pH 7.5, 150 mM NaCl. Liposomes at a final concentration of 1 mg ml^{-1} were incubated with 20 µM protein for 10 min at room temperature in a 40 µl reaction volume, followed by a 200,000*g* spin for 10 min at 20 °C (see also http://www.endocytosis.org). The Liposome binding competition assay was performed at final concentration of 10 µM and 50 µM $CaCl_2$ or 700 µM IP3 (1,4,5; Sigma) dissolved in Liposome solubilization buffer. The intensity of the SDS bends were quantitatively analyzed using the Image Lab Software suite (BioRad).

Shiga toxin (STX) and Cholera toxin (CTX) uptake assays. Upon siRNA revers transfection, cells were plated on glass coverslips to reach 70%–80% confluency on the day of the experiment AF647 labeled Shiga toxin or Cholera toxin B subunit (final concentration 5 µg/ml) was diluted in the serum free DMEM

and centrifuged for 5 min at 14,000 rpm to clarify the solution. Cells were incubated with Shiga or Cholera toxin for 45 min at 37 °C (coverslips upside down), washed three times with PBS and fixed using 4% PFA/4% sucrose for 30min at RT. Images were acquired with EPI microscope and Fluorescence intensities per cell were quantified using ImageJ.

GM1 loading assay. Cells were incubated with exogenous GM1 (final concentration: 5 µM GM1) in 10%FCS/ DMEM for 4 h at 37 °C. After 4 hours medium was replaced with 10%FCS/ DMEM and cells were incubated at 37 °C for another 4 h.

EGF, transferrin, and wheat germ agglutinin (WGA) surface labelling and uptake assays. Cells were plated on glass coverslips to reach 70–80% confluency on the day of the experiment. Cells were starved in serum free DMEM for 1h and 3h, respectively but for WGA surface labelling cells were not starved. For surface labelling cells (coverslips upside down) were incubated with Tf-Alexa Fluor 647 (25 µg/ml in serum free DMEM), EGF-Alexa Fluor 647 (500 ng/ml in serum free DMEM) and WGA Alexa Fluor 647 (2.5 µg/ml in HBSS) for 45 min at 4°C (incubation chambers on ice in the cold room), washed three times with ice cold PBS. For Tf and EGF uptake, cells were incubated with Tf-Alexa Fluor 647 (25 µg/ml) and EGF-Alexa Fluor 647 (500 ng/ml) for 10 min (Tf) or 30 min (EGF) at 37°C. Next, cells were washed with ice cold PBS and non endocytosed ligand, still bound to the surface, was removed by acid wash (0.2 M NaCl, 0.1 M NaOAc pH 5.3, 1min on ice). Cells were washed twice with ice cold PBS. All samples were fixed using ice-cold 4% PFA/4% sucrose for 45 min at RT. Images were acquired with EPI microscope and Fluorescence intensities per cell were quantified using ImageJ.

Lipidomic analyses

Cells were subjected to lipid extractions using an acidic Bligh and Dyer liquid-liquid extraction method[67], except from plasmalogens, which were extracted under neutral conditions. Lipid standards were added prior to extractions, using a master mix containing 50 pmol phosphatidylcholine (PC, 13:0/13:0, 14:0/14:0, 20:0/20:0; 21:0/21:0, Avanti Polar Lipids), 50 pmol sphingomyelin (SM, d18:1 with N-acylated 13:0, 17:0, 25:0, semi-synthesized)[68], 100 pmol cholesterol (Chol)-D_6 (Cambrigde Isotope Laboratory), 30 pmol phosphatidylinositol (PI, 16:0/ 16:0, Avanti Polar Lipids), 25 pmol phosphatidylethanolamine (PE) and 25 pmol phosphatidylserine (PS) (both 14:1/14:1, 20:1/20:1, 22:1/22:1, semi-synthesized)[68], 25 pmol diacylglycerol (DAG, 17:0/17:0, Larodan), 20/25 pmol cholesterol ester (CE, 9:0, 19:0, 24:1, Sigma), and 24 pmol triacylglycerol (TAG, LM–6000/D5–17:0,17:1,17:1, Avanti Polar Lipids), 5 pmol ceramide (Cer) and 5 pmol glucosylceramide (HexCer) (both d18:1 with N-acylated 15:0, 17:0, 25:0, semi-synthesized)[68], 5 pmol lactosylceramide (Hex2Cer, d18:1 with N-acylated C12 fatty acid), 10 pmol phosphatidic acid (PA, 21:0/22:6, Avanti Polar), 10 pmol phosphatidylglycerol (PG, 14:1/14:1, 20:1/20:1, 22:1/22:1, semi-synthesized)[68] and 5 pmol lysophosphatidylcholine (LPC, 17:1, Avanti Polar Lipids). Phosphatidylethanolamine plasmalogen (PE P-)-containing standard mix was supplemented with 16.5 pmol PE P-Mix 1 (16:0p/15:0, 16:0p/19:0, 16:0p/ 25:0), 23.25 pmol PE P- Mix 2 (18:0p/15:0, 18:0p/19:0, 18:0p/25:0), 32.25 pmol PE P-Mix 3 (18:1p/15:0, 18:1p/19:0, 18:1p/25:0). Semi-synthesis of PE P- was performed as described in[69]. The final chloroform phase was evaporated under a gentle stream of

nitrogen. Lipid extracts were resuspended in 60 µl methanol and samples were analyzed on an QTRAP 6500 + mass spectrometer (Sciex) with chip-based (HD-D ESI Chip, Advion Biosciences) electrospray infusion and ionization via a Triversa Nanomate (Advion Biosciences) as described[68]. Resuspended lipid extracts were diluted 1:10 in 96-well plates (Eppendorf twin tec 96) prior to measurement. Data evaluation was done using LipidView (Sciex) and an in-house-developed software (ShinyLipids).

LC-MS based glycosphingolipid analysis. Extraction of glycosphingolipids and gangliosides was performed as described in[70] . Briefly, the sample amount was adjusted to eight times the amount used for direct injection. The sample volume was adjusted to 200 µL using 155 mM ammonium bicarbonate buffer. A first neutral extraction was performed using chloroform:methanol (17:1, vol:vol), followed by a chloroform:methanol (2:1, vol:vol) extraction. The following internal standards (Matreya LLC) were used: 25 pmol GB3 (d18:1/18:0-D_3), 25 pmol GM3 (d18:1/18:0-D_3), 25 pmol GM1 (d18:1/18:0-D_3) and 25 pmol GD1 (d18:1/18:0-D_3) semi-synthesized in-house based on. For analysis of GM1 and GD1 the remaining aqueous phase was purified with C8 functionalized solid-phase extraction. Following evaporation of the organic solvent, lipid extracts were resuspended in 100 µl mobile phase containing 60% of acetonitrile:water, (60:40, vol:vol) in 10 mM ammonium formate and 0.1% formic acid (mobile phase A) and 40% isopropanol:acetonitrile (90:10, vol:vol) in 10 mM ammonium formate and 0.1% formic acid (mobile phase B) and transferred to silanized glass inlets, positioned in 2 mL glass vials with PTFE coated caps. Glycosphingolipids were subjected to UHPLC-MS analysis at a flow rate of 0.1 mL/min, using a CSH C18 column (1x150mm, 1.7 µm particles, Waters) coupled to a QExactive Q/orbitrap tandem-MS (Thermo Scientific) equipped with an ESI source. Measurement in positive and negative ion mode was performed including switching between Full-MS and All ions fragmentation (AIF). For one injection 12.5 µL of each sample was subjected to UPLC separation (Dionex), using a step gradient of 60–50% A (0.0–3.0 min), 50–46% A (3.0–9.0 min), 46–30% A (9.0–9.1 min), 30–10% A (9.1–17.0 min), 10% A (17.0–22.0 min), 10–60% A (22.0–22.5 min) and 60% A (22.5–30.0 min). The column temperature was set to 55°C and the flow rate to 0.1 mL/min. Full MS scans were acquired for 25 min in positive and negative ion mode (m/z 500–1,800) were with automatic gain control (AGC) target of $3x10^6$ ions, maximal injection time of 200 ms and resolution set to 140,000. AIF in positive and negative ion mode was performed with AGC target of $1x10^6$ ions, scanning a mass range of 120–600 m/z with normalised collision energy set to 30 eV. Data evaluation of Full-MS scans (profile spectra) was performed using MassMap.

Light microscopy of cultured cells. Treated cells were washed once with PBS, fixed with 4% PFA/4% sucrose for 20 min at RT. Washed three times with PBS–10 mM $MgCl_2$ and blocked/permeabilized with GSDB [10% Goat serum, 100mM NaCl, 0.3% Triton X–100, in PBS] for 30 min at RT. Primaries antibodies were diluted in GSDB and applied for 2h at RT. Next cells were washed three times with PBS–10 mM $MgCl_2$ and incubated with appropriate Alexa Conjugated secondary antibodies diluted in GSDB. Cells were washed three times with PBS–10 mM $MgCl_2$, diped in the water and mounted with immunomount supplemented with DAPI. Images were acquired with a minimum resolution (512px x 512px) for confocal

imaging using Zeiss LSM 710 or LSM780 microscopes. Images analysis and quantification were performed using FIJI.

Measurements of intracellular calcium levels. Calcium levels at the steady state were measured in HeLaM cells treated with control or INPP5A siRNA. Cells were incubated with 2mM Fluo–4/0.02% pluronic for 10 min in serum free DMEM. Then cells were washed three times with PBS supplemented with Calcium and Mg2+. Cells were imaged life in PBS and images were acquired with LSM.

Phosphoinositide staining. Cells were washed with PBS–10 mM $MgCl_2$, fixed with 2% PFA/2% sucrose/PBS for 20 min and permeablised with 0.5% Saponin (in PBS/1% BSA) for 30 min at RT. Then cells were incubated with anti-PI4P or PI(4,5)P2 antibodies diluted in PBS/1% BSA for 2 h at RT. After three washes with PBS–10 mM $MgCl_2$, cells were incubated with goat anti mouse igM AF568 diluted in PBS/1% BSA. Cells were washed three times with PBS–10 mM $MgCl_2$ and mounted with immomount supplemented with DAPI.

Lipid droplet staining. cells were revers transfected with negative control siRNA or siRNA against INPP5A, then seeded over a Matrigel-coated cover glass for 48 hours and incubated in 5% CO2 at 37°C. Then cells were washed twice with PBS and incubated with for 15 min with 2u M BODYPI 493/503 (4,4-Difluoro–1,3,5,7,8-Pentamethyl–4-Bora–3a,4a-Diaza-s-Indacene) before they are fixed with 4% PFA/4% sucrose for 30 min at room temperature (RT). Cells were washed three times with PBS–10 mM $MgCl_2$ and mounted with immomount supplemented with DAPI.

Filipin staining. HeLa cells were transfected with negative control siRNA or siRNA against INPP5A, then seeded onto Matrigel-coated cover glass for 48 hours and incubated in 5% CO_2 at 37°C. Cells were washed twice with PBS and fixed with 4% PFA/ 4% sucrose for 60 min at RT. Cells were washed three times with PBS and incubated with 1.5 mg/ ml glycine in PBS for 10 min, then incubated in a dark room with the Filipin working solution for two hours. Samples were rinsed three times with PBSand imaged live by epifluorescence microscopy using a UV filter set (340–380 excitation, 40 nm dichroic, 430-nm long pass filter).

Immunoprecipitation. HEK293T cells co-transfected with OSBP-GFP and VAPA-HA were washed three times in PBS and lysed in immunoprecipitation (IP) buffer (20 mM HEPES, pH 7.4, 130 mM NaCl, 0.3% protease inhibitor cocktail (Sigma-Aldrich), 10 mM NaF, phosphatase inhibitors (cocktails 2 and 3, Sigma-Aldrich) and 1% NP–40). Samples were centrifuged at 10,000g for 10 min at 4 °C, and the supernatant was then incubated with HA-Trap magnetic microparticles (ChromoTek) for 1 h at 4 °C. Beads were washed three times with IP buffer, and bound proteins were eluted in SDS–PAGE sample buffer, resolved by SDS–PAGE and analysed via immunoblot.

Cell lysates and immunoblotting. Cells were washed three times in ice-cold PBS and collected in PBS with 1% Triton X–100, 0.3% protease inhibitor cocktail (Sigma-Aldrich) and phosphatase inhibitors (cocktails 2 and 3, Sigma-Aldrich). Protein levels were quantified using Bradford reagent (Sigma-Aldrich). Equal

concentration lysates in Laemmli sample buffer were boiled for 5 min; between 10 and 50 µg protein was resolved by SDS–PAGE and analysed via immunoblot using LI-COR 800CW and 680RD infrared secondary antibodies as indicated.

*Statistics and reproducibility.*Values are depicted as mean ± SEM or mean ± SD as indicated in the figure legends. One-sample two-sided t-tests were used for comparisons with control group values that had been set to 1 for normalization purposes and that therefore did not fulfill the requirement of two-sample t-tests or one-way ANOVA concerning the homogeneity of variances. The Benjamini-Hochberg procedure was used to correct for multiple testing based on the acceptance of a false discovery rate of 5% (see figure legends). GraphPad Prism version 8 software was used for statistical analysis. The level of significance is indicated in the figures by asterisks (* = p0.05; ** = p0.01; *** = p0.001; **** = p0.0001) and provided in the figure legends as exact p-value as obtained by the indicated statistic test. No statistical method was used to pre-determine sample size as sample sizes were not chosen based on pre-specified effect size. Instead, multiple independent experiments were carried out using several sample replicates as detailed in the figure legends.

Declarations

Acknowledgements

We are indebted to Drs. Pietro De Camilli (Yale University School of Medicine HHMI, New Haven, CT, USA) for the kind gift of VAP-A/B double KO HeLa cells, Maria Antonella De Matteis (Telethon Institute of Genetics and Medicine-TIGEM, Pozzuoli, Italy) for antibodies against OSBP, and Caspar C. Hoogenraad (Utrecht University, Utrecht, The Netherlands) and Greg Fairn (St. Michael's Hospital, Unity Health Toronto, Canada) for plasmids. We wish to thank Maria Mühlbauer, Silke Zillmann, and Delia Löwe for technical assistance.

Supported by grants from the Leibniz SAW Program (to V. H.), the Deutsche Forschungsgemeinschaft (TRR186/A08 to V. H. and TRR186/A05 to B. B.), and the Fonds für Wissenschaftliche Forschung (FWF, Austria; to M. H.).

Author contributions

P. K. conducted the initial siRNA screen, M. M., A. W., and W. J. performed most biochemical and cell biological experiments, C. L., T. S. and B. B. conducted the lipidomic analysis, M. H. analyzed PH domain binding to PI(4)P-containing liposomes. V. H. designed the study and together with M. M. wrote the manuscript with input from all authors.

Competing interests

The authors declare no competing interests.

Materials & Correspondence

Requests for materials and correspondence should be addressed to: V. H. (haucke@fmp-berlin.de).

Data availability

The data that support these findings are available from the authors on request. Numerical source data for Figs. 1–6 and uncropped versions of blots and gels are provided in the Source Data File.

References

1.De Camilli P, Emr SD, McPherson PS, Novick P. Phosphoinositides as regulators in membrane traffic. *Science 271,* 1533–1539 (1996).

2.Rothman JE, Wieland FT. Protein sorting by transport vesicles. *Science 272,* 227–234 (1996).

3.Bohnert M, Schuldiner M. Stepping outside the comfort zone of membrane contact site research. *Nat Rev Mol Cell Biol 19,* 483–484 (2018).

4.Prinz WA, Toulmay A, Balla T. The functional universe of membrane contact sites. *Nat Rev Mol Cell Biol 21,* 7–24 (2020).

5.Saheki Y, De Camilli P. Endoplasmic Reticulum-Plasma Membrane Contact Sites. *Annu Rev Biochem 86,* 659–684 (2017).

6.Scorrano L*, et al.* Coming together to define membrane contact sites. *Nat Commun 10,* 1287 (2019).

7.Wu H, Carvalho P, Voeltz GK. Here, there, and everywhere: The importance of ER membrane contact sites. *Science 361,* (2018).

8.Burgoyne T, Patel S, Eden ER. Calcium signaling at ER membrane contact sites. *Biochim Biophys Acta 1853,* 2012–2017 (2015).

9.Collins SR, Meyer T. Evolutionary origins of STIM1 and STIM2 within ancient Ca2+ signaling systems. *Trends Cell Biol 21,* 202–211 (2011).

10.Venditti R, Masone MC, De Matteis MA. ER-Golgi membrane contact sites. *Biochem Soc Trans 48,* 187–197 (2020).

11.Mesmin B, Bigay J, Polidori J, Jamecna D, Lacas-Gervais S, Antonny B. Sterol transfer, PI4P consumption, and control of membrane lipid order by endogenous OSBP. *EMBO J 36,* 3156–3174 (2017).

12.Peretti D, Dahan N, Shimoni E, Hirschberg K, Lev S. Coordinated lipid transfer between the endoplasmic reticulum and the Golgi complex requires the VAP proteins and is essential for Golgi-mediated transport. *Mol Biol Cell 19,* 3871–3884 (2008).

13.Wyles JP, McMaster CR, Ridgway ND. Vesicle-associated membrane protein-associated protein-A (VAP-A) interacts with the oxysterol-binding protein to modify export from the endoplasmic reticulum. *J Biol Chem 277,* 29908–29918 (2002).

14.Ikonen E. Mechanisms of cellular cholesterol compartmentalization: recent insights. *Curr Opin Cell Biol 53,* 77–83 (2018).

15.Simons K, Ikonen E. Functional rafts in cell membranes. *Nature 387,* 569–572 (1997).

16.Ding X, Zhang W, Li S, Yang H. The role of cholesterol metabolism in cancer. *Am J Cancer Res 9,* 219–227 (2019).

17.Harder T, Scheiffele P, Verkade P, Simons K. Lipid domain structure of the plasma membrane revealed by patching of membrane components. *J Cell Biol 141,* 929–942 (1998).

18.Nichols BJ. GM1-containing lipid rafts are depleted within clathrin-coated pits. *Curr Biol 13,* 686–690 (2003).

19.Pichler H, Riezman H. Where sterols are required for endocytosis. *Biochim Biophys Acta 1666,* 51–61 (2004).

20.Skotland T, Kavaliauskiene S, Sandvig K. The role of lipid species in membranes and cancer-related changes. *Cancer Metastasis Rev,* (2020).

21.Lingwood D, Ries J, Schwille P, Simons K. Plasma membranes are poised for activation of raft phase coalescence at physiological temperature. *Proc Natl Acad Sci U S A 105,* 10005–10010 (2008).

22.Lakshminarayan R*, et al.* Galectin–3 drives glycosphingolipid-dependent biogenesis of clathrin-independent carriers. *Nat Cell Biol 16,* 595–606 (2014).

23.Falguieres T*, et al.* Targeting of Shiga toxin B-subunit to retrograde transport route in association with detergent-resistant membranes. *Mol Biol Cell 12,* 2453–2468 (2001).

24.Romer W*, et al.* Actin dynamics drive membrane reorganization and scission in clathrin-independent endocytosis. *Cell 140,* 540–553 (2010).

25.Windschiegl B*, et al.* Lipid reorganization induced by Shiga toxin clustering on planar membranes. *PLoS One 4,* e6238 (2009).

26.Renard HF*, et al.* Endophilin-A2 functions in membrane scission in clathrin-independent endocytosis. *Nature 517,* 493–496 (2015).

27.Boucrot E*, et al.* Endophilin marks and controls a clathrin-independent endocytic pathway. *Nature 517,* 460–465 (2015).

28.Ferreira APA, Boucrot E. Mechanisms of Carrier Formation during Clathrin-Independent Endocytosis. *Trends Cell Biol 28,* 188–200 (2018).

29.Horne JH, Meyer T. Elementary calcium-release units induced by inositol trisphosphate. *Science 276,* 1690–1693 (1997).

30.Taylor CW, Machaca K. IP3 receptors and store-operated Ca(2+) entry: a license to fill. *Curr Opin Cell Biol 57,* 1–7 (2019).

31.Koenig S, Moreau C, Dupont G, Scoumanne A, Erneux C. Regulation of NGF-driven neurite outgrowth by Ins(1,4,5)P3 kinase is specifically associated with the two isoenzymes Itpka and Itpkb in a model of PC12 cells. *FEBS J 282,* 2553–2569 (2015).

32.Berridge MJ. The Inositol Trisphosphate/Calcium Signaling Pathway in Health and Disease. *Physiol Rev 96,* 1261–1296 (2016).

33.Patel AB*, et al.* Frequent loss of inositol polyphosphate–5-phosphatase in oropharyngeal squamous cell carcinoma. *J Eur Acad Dermatol Venereol 32,* e36-e37 (2018).

34.Speed CJ, Little PJ, Hayman JA, Mitchell CA. Underexpression of the 43 kDa inositol polyphosphate 5-phosphatase is associated with cellular transformation. *EMBO J 15,* 4852–4861 (1996).

35.Speed CJ, Neylon CB, Little PJ, Mitchell CA. Underexpression of the 43 kDa inositol polyphosphate 5-phosphatase is associated with spontaneous calcium oscillations and enhanced calcium responses following endothelin–1 stimulation. *J Cell Sci 112 (Pt 5),* 669–679 (1999).

36.Communi D, Lecocq R, Erneux C. Arginine 343 and 350 are two active residues involved in substrate binding by human Type I D-myo-inositol 1,4,5,-trisphosphate 5-phosphatase. *J Biol Chem 271,* 11676–11683 (1996).

37.Liu Q*, et al.* Cerebellum-enriched protein INPP5A contributes to selective neuropathology in mouse model of spinocerebellar ataxias type 17. *Nat Commun 11,* 1101 (2020).

38.Giordano F*, et al.* PI(4,5)P(2)-dependent and Ca(2+)-regulated ER-PM interactions mediated by the extended synaptotagmins. *Cell 153,* 1494–1509 (2013).

39.Balla T. Phosphoinositides: tiny lipids with giant impact on cell regulation. *Physiol Rev 93,* 1019–1137 (2013).

40.Wang H*, et al.* Phosphatidylinositol 3,4-bisphosphate synthesis and turnover are spatially segregated in the endocytic pathway. *J Biol Chem 295,* 1091–1104 (2020).

41.Gozzelino L, De Santis MC, Gulluni F, Hirsch E, Martini M. PI(3,4)P2 Signaling in Cancer and Metabolism. *Front Oncol 10,* 360 (2020).

42.Speed CJ, Mitchell CA. Sustained elevation in inositol 1,4,5-trisphosphate results in inhibition of phosphatidylinositol transfer protein activity and chronic depletion of the agonist-sensitive phosphoinositide pool. *J Cell Sci 113 (Pt 14),* 2631–2638 (2000).

43.Torgersen ML, Skretting G, van Deurs B, Sandvig K. Internalization of cholera toxin by different endocytic mechanisms. *J Cell Sci 114,* 3737–3747 (2001).

44.Brugger B, Glass B, Haberkant P, Leibrecht I, Wieland FT, Krausslich HG. The HIV lipidome: a raft with an unusual composition. *Proc Natl Acad Sci U S A 103,* 2641–2646 (2006).

45.Brugger B, Erben G, Sandhoff R, Wieland FT, Lehmann WD. Quantitative analysis of biological membrane lipids at the low picomole level by nano-electrospray ionization tandem mass spectrometry. *Proc Natl Acad Sci U S A 94,* 2339–2344 (1997).

46.Xu YH, Barnes S, Sun Y, Grabowski GA. Multi-system disorders of glycosphingolipid and ganglioside metabolism. *J Lipid Res 51,* 1643–1675 (2010).

47.Gkantiragas I*, et al.* Sphingomyelin-enriched microdomains at the Golgi complex. *Mol Biol Cell 12,* 1819–1833 (2001).

48.Fujita A, Cheng J, Hirakawa M, Furukawa K, Kusunoki S, Fujimoto T. Gangliosides GM1 and GM3 in the living cell membrane form clusters susceptible to cholesterol depletion and chilling. *Mol Biol Cell 18,* 2112–2122 (2007).

49.Maekawa M, Yang Y, Fairn GD. Perfringolysin O Theta Toxin as a Tool to Monitor the Distribution and Inhomogeneity of Cholesterol in Cellular Membranes. *Toxins (Basel) 8,* (2016).

50.Mesmin B, Bigay J, Moser von Filseck J, Lacas-Gervais S, Drin G, Antonny B. A four-step cycle driven by PI(4)P hydrolysis directs sterol/PI(4)P exchange by the ER-Golgi tether OSBP. *Cell 155,* 830–843 (2013).

51.Venditti R*, et al.* Molecular determinants of ER-Golgi contacts identified through a new FRET-FLIM system. *J Cell Biol 218,* 1055–1065 (2019).

52.Dong R, Saheki Y, Swarup S, Lucast L, Harper JW, De Camilli P. Endosome-ER Contacts Control Actin Nucleation and Retromer Function through VAP-Dependent Regulation of PI4P. *Cell 166,* 408–423 (2016).

53.Erneux C, Ghosh S, Koenig S. Inositol(1,4,5)P3 3-kinase isoenzymes: Catalytic properties and importance of targeting to F-actin to understand function. *Adv Biol Regul 60,* 135–143 (2016).

54.Shears SB. How versatile are inositol phosphate kinases? *Biochem J 377,* 265–280 (2004).

55.Williams RS, Eames M, Ryves WJ, Viggars J, Harwood AJ. Loss of a prolyl oligopeptidase confers resistance to lithium by elevation of inositol (1,4,5) trisphosphate. *EMBO J 18,* 2734–2745 (1999).

56.Kang JK*, et al.* Increased intracellular Ca(2+) concentrations prevent membrane localization of PH domains through the formation of Ca(2+)-phosphoinositides. *Proc Natl Acad Sci U S A 114,* 11926–11931 (2017).

57.Balla A, Tuymetova G, Tsiomenko A, Varnai P, Balla T. A plasma membrane pool of phosphatidylinositol 4-phosphate is generated by phosphatidylinositol 4-kinase type-III alpha: studies with the PH domains of the oxysterol binding protein and FAPP1. *Mol Biol Cell 16,* 1282–1295 (2005).

58.Yang AW, Sachs AJ, Nystuen AM. Deletion of Inpp5a causes ataxia and cerebellar degeneration in mice. *Neurogenetics 16,* 277–285 (2015).

59.D'Angelo G*, et al.* Glycosphingolipid synthesis requires FAPP2 transfer of glucosylceramide. *Nature 449,* 62–67 (2007).

60.Maeda Y*, et al.* Effects of cyclodextrins on GM1-gangliosides in fibroblasts from GM1-gangliosidosis patients. *J Pharm Pharmacol 67,* 1133–1142 (2015).

61.Eden ER, Sanchez-Heras E, Tsapara A, Sobota A, Levine TP, Futter CE. Annexin A1 Tethers Membrane Contact Sites that Mediate ER to Endosome Cholesterol Transport. *Dev Cell 37,* 473–483 (2016).

62.Campbell JK*, et al.* Activation of the 43 kDa inositol polyphosphate 5-phosphatase by 14–3–3zeta. *Biochemistry 36,* 15363–15370 (1997).

63.Renard HF*, et al.* Endophilin-A3 and Galectin–8 control the clathrin-independent endocytosis of CD166. *Nat Commun 11,* 1457 (2020).

64.Garcia-Ruiz C, Morales A, Fernandez-Checa JC. Glycosphingolipids and cell death: one aim, many ways. *Apoptosis 20,* 607–620 (2015).

65.Gallego-Iradi C*, et al.* KCNC3(R420H), a K(+) channel mutation causative in spinocerebellar ataxia 13 displays aberrant intracellular trafficking. *Neurobiol Dis 71,* 270–279 (2014).

66.Sharkey LM*, et al.* The ataxia3 mutation in the N-terminal cytoplasmic domain of sodium channel Na(v)1.6 disrupts intracellular trafficking. *J Neurosci 29,* 2733–2741 (2009).

67.Bligh EG, Dyer WJ. A rapid method of total lipid extraction and purification. *Can J Biochem Physiol 37,* 911–917 (1959).

68.Ozbalci C, Sachsenheimer T, Brugger B. Quantitative analysis of cellular lipids by nano-electrospray ionization mass spectrometry. *Methods Mol Biol 1033,* 3–20 (2013).

69.Paltauf F, Hermetter A. Strategies for the synthesis of glycerophospholipids. *Prog Lipid Res 33,* 239–328 (1994).

70.Ejsing CS, *et al.* Global analysis of the yeast lipidome by quantitative shotgun mass spectrometry. *Proc Natl Acad Sci U S A 106,* 2136–2141 (2009).

Figures

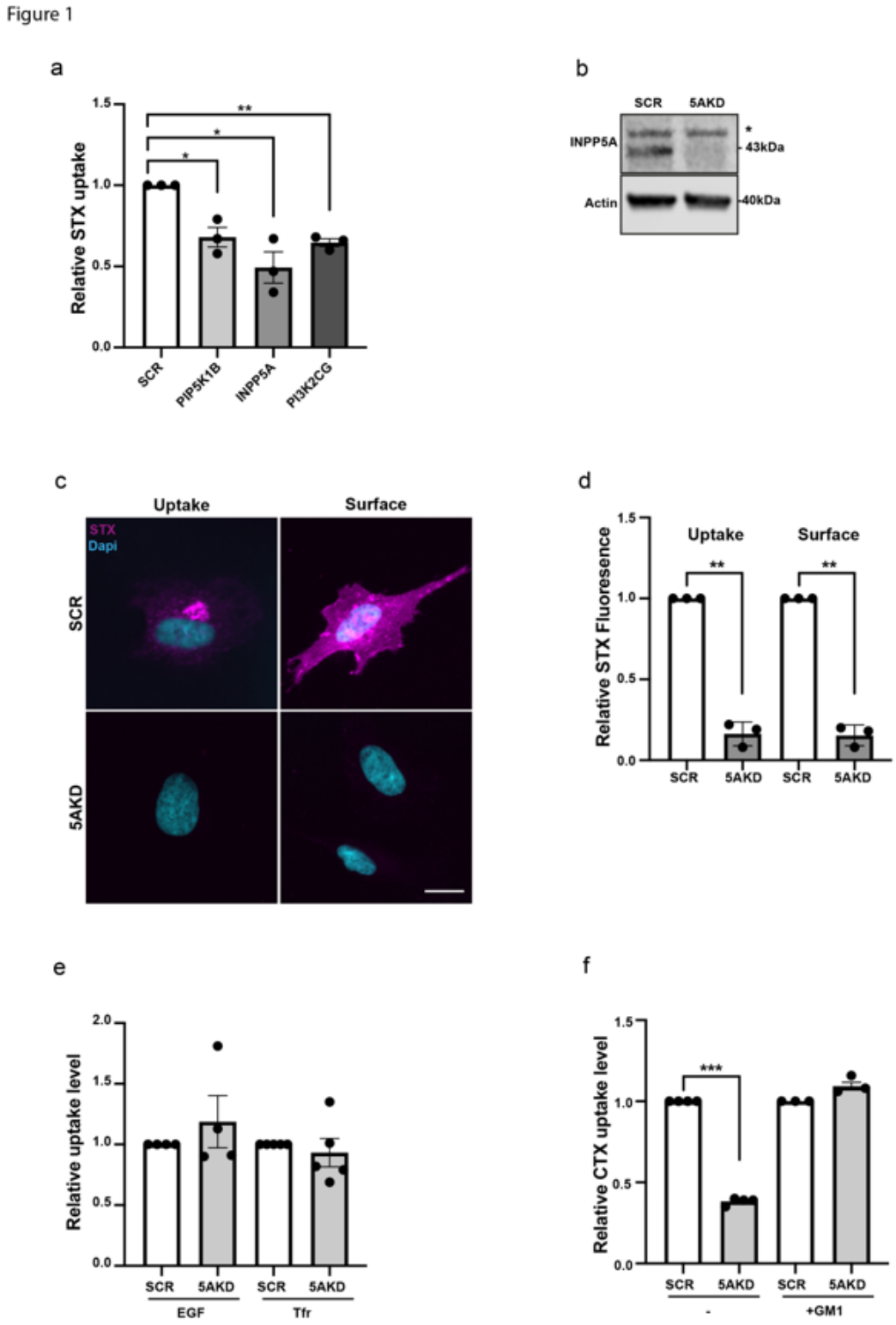

Figure 1

INPP5A loss impairs clathrin-independent endocytosis of bacterial toxins by destabilizing surface glycosphingolipids. (a) Relative Shiga toxin (STX; 5 µg/ml) uptake in HeLa cells treated with smart pool siRNAs against the indicated proteins. STX uptake into SCR-siRNA-treated control cells was set to 1. STX uptake was reduced in cells depleted of INPP5A, PIP5K1B, or PI3KC2γ (PI3K2CG). Data are from n=3 independent experiments. One sample student's t-test followed by Benjamini Hochberg correction: PIP5K1B : p = 0.0343, t = 5.261, df = 2. INPP5A: p = 0.0343, t = 5.279, df = 2. PI3K2CG : p = 0.0138, t = 14.7, df = 2. (b) Representative immunoblot analysis of HeLa cells treated with control (SCR) or INPP5A siRNA (5AKD). Immunoblots were decorated with antibodies against INPP5A and β-actin as a loading control. Asterisk denotes a non-specific background band decorated by INPP5A antibodies. (c) Representative confocal images of HeLa cells treated with control (SCR) or INPP5A siRNA (5AKD) and incubated with labeled STX (magenta). Cells were either incubated at 37°C for 15 min or kept at 4°C for 45 min to measure endocytosis (uptake) or surface binding (surface), respectively. Blue, DAPI-stained nuclei. Scale bar, 25 µm. (d) Quantification of representative data shown in (c). Data for SCR-control siRNA-treated cells were set to 1. One sample student's t-test for each pair. Uptake : p = 0.0026 , t = 19.66 , df = 2 . Surface : p = 0.0019 , t = 22.81 , df =2. (e) Relative uptake of EGF or transferrin in HeLa cells treated with control (SCR, set to 1) or INPP5A siRNA (5AKD). One sample student's t-test, EGF : p = 0.4458, t = 0.8754, df = 3. Trf : p = 0.5912, t = 0.5830, df = 3. (f) Relative Cholera-Toxin (CTX) uptake in HeLa cells treated with the indicated smart pool siRNAs. Data for SCR-control siRNA-treated cells with or without GM1were set to 1. Defective CTX endocytosis was rescued by overnight incubation with the Ganglioside GM1. Data represent mean ± SEM from at least n=3 independent experiments. One sample student's t-test for each pair. 5AKD: p = <0.0001 , t = 55.7 , df =3 . ITPKBKD: p = <0.0001 , t = 119 , df =2 . GM1+5AKD : p = <0.0604 , t = 3.883 , df =2. All data represent mean ± SEM from at least 3 independent experiments. Numerical source data and unprocessed blots are reported in the Source Data file.

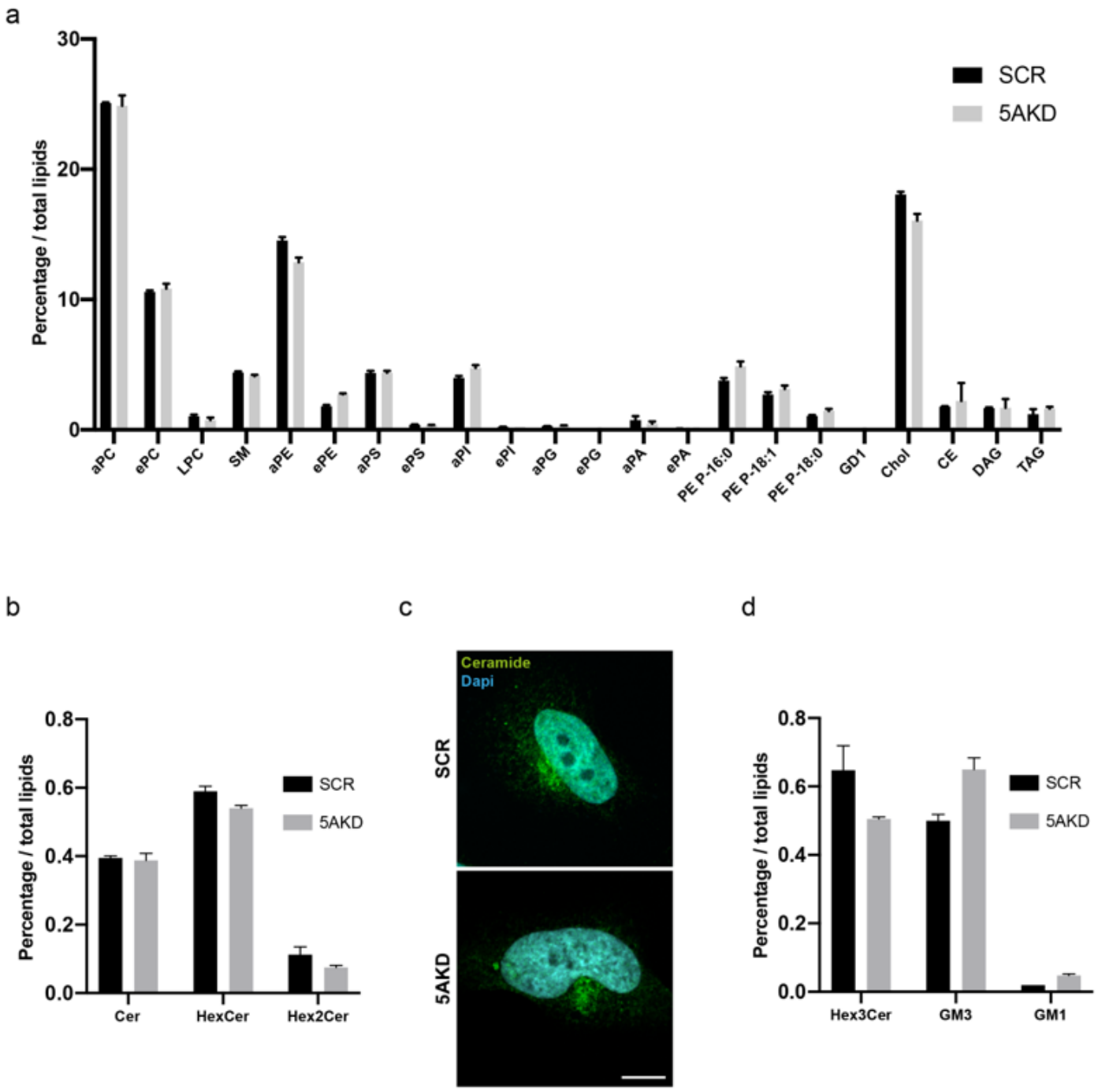

Figure 2

Unaltered cellular lipid levels in absence of INPP5A. (a,b,d) Lipidomic analyses of control (scrambled siRNA, SCR) and INPP5A-depleted (1.0 x 106) HeLa cells. ceramide (Cer), cholesterol (Chol), cholesteryl ester (CE), diacylglycerol (DAG), dihexosylceramide (Hex2Cer), ganglioside GD1 (GD1), ganglioside GM1 (GM1), ganglioside GM3 (GM3), globoside GB3 (trihexosylceramide, Hex3Cer), hexosylceramide (HexCer), lyso-PC (LPC), phosphatidic acid (PA), phosphatidylcholine (PC), phosphatidylethanolamine (PE), phosphatidylglycerol (PG), phosphatidyinositol (PI), phosphatidylserine (PS), plasmalogen (plasmenyl) ethanolamine (PE-P), sphingomyelin (SM), triacylglycerol (TAG), trihexosylceramide (HexCer, GB3). Prefix a indicates acyl-linked glycerophospholipids, prefix e indicates ether-linked (plasmanyl) or containing one

odd chain fatty acyl. Data represent mean ± SEM from at least n=4 independent experiments. A t-test was performed. aPC : p =0.63, t=0.49, df = 6. ePC : p =0.21, t=1.40, df = 6. LPC : p =0.04, t=2.574, df = 6. SM: p =0.01, t=3.63, df = 6.aPE: p =0.0002, t=7.70, df = 6. ePE : p =0.000006, t=,14.65, df = 6. aPS: p =0.9, t=,0.11 df = 6. ePS : p =0.01, t=3.70, df = 6. aPI : p =0.001, t=5.82, df = 6. ePI: p =0.77, t=0.29, df = 6. aPG: p =,0.0003 t=7.38, df = 6. aPa : p =0.134, t=1.72, df = 6. ePA : p =0.07, t=2.18, df = 6. pl-PE 16:0: p =0.002, t=5.08, df = 6. pl-PE 18:1: p =0.044, t=2.52, df = 6. pl-PE 18:0: p =0.004, t=4.51, df = 6. Chlesterol: p =0.0003, t=7.28, df = 6. CE : p =0.544, t=0.64, df = 6.DAG : p =0.89, t=0.14, df = 6.TAG: p =0.07, t=2.12, df = 6.Cer: p =0.509, t=0.7, df = 6.HexCer: p =0.0008, t=,6.12 df = 6.Hex2Cer: p =0.016, t=3.27, df = 6.Hex3Cer: p =0.007, t=3.95, df = 6.GM3: p =0.0002, t=7.83, df = 6.GM1: p =0.000034, t=11, df = 6. (c) Representative confocal images of HeLa cells treated with control (SCR) or INPP5A siRNA (5AKD) and incubated with Ceramide antibody (green). Blue, DAPI-stained nuclei. Scale bar, 10 μm. Numerical source data and unprocessed blots are reported in the Source Data file.

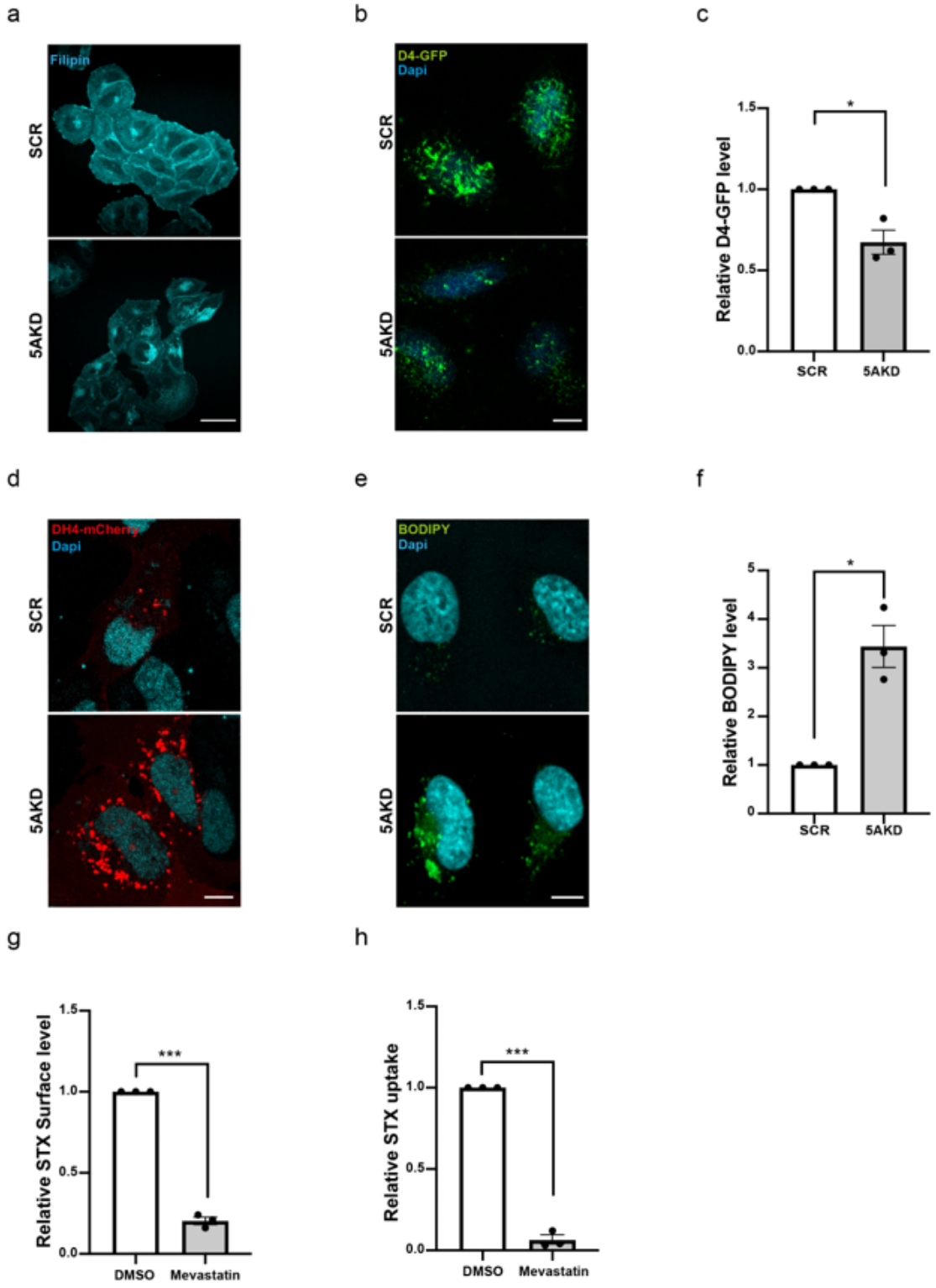

Figure 3

Cholesterol is depleted from the cell surface and re-routed to lipid droplets in the absence of INPP5A. (a) Representative epifluorescent images of HeLa cells treated with control (SCR) or INPP5A siRNA (5AKD) and incubated for 45 min post-fixation with 0.05 mg/ml Filipin (cyan). Scale bar, 25 μm. (b,d) Representative confocal images of HeLa cells treated with control (SCR) or INPP5A siRNA (5AKD) and (b) stained for plasma membrane cholesterol using recombinant D4-GFP (green) or (d) transfected with a

plasmid encoding DH4-mCherry (red) to detect intracellular cholesterol. Blue, DAPI-stained nuclei. Scale bar, 10 µm. (c) Relative D4-GFP level as a measure for plasma membrane cholesterol in HeLa cells treated with control (SCR) or INPP5A siRNA (5AKD). One sample student's t-test 5AKD: p =0.048, t =4.4 , df =2.(e) Representative images of HeLa cells treated with control (SCR) or INPP5A siRNA (5AKD) and incubated for 15 min with 2 M of BODIPY™ 493/503 (4,4-Difluoro-1,3,5,7,8-Pentamethyl-4-Bora-3a,4a-Diaza-s-Indacene) (green) before fixation. Scale bar, 10 µm (f) Relative BODIPY™ levels as a measure for lipid droplets in HeLa cells treated with control (SCR) or INPP5A siRNA (5AKD). One sample student's t-test 5AKD: p = 0.03, t = 5.642 , df = 2. (g) Relative STX surface level in HeLa cells treated with DMSO or depleted of cholesterol by treatment with 250 nM of the HMG-CoA reductase inhibitor Mevastatin for 24 h. One sample student's t-test : p =0.0009, t =34.14, df =2. (h) Relative STX uptake in HeLa cells treated with DMSO or depleted of cholesterol by treatment with 250 nM of the HMG-CoA reductase inhibitor Mevastatin for 24 h. One sample student's t-test : p = 0.0009, t = 32.89 , df = 2. Numerical source data and unprocessed blots are reported in the Source Data file.

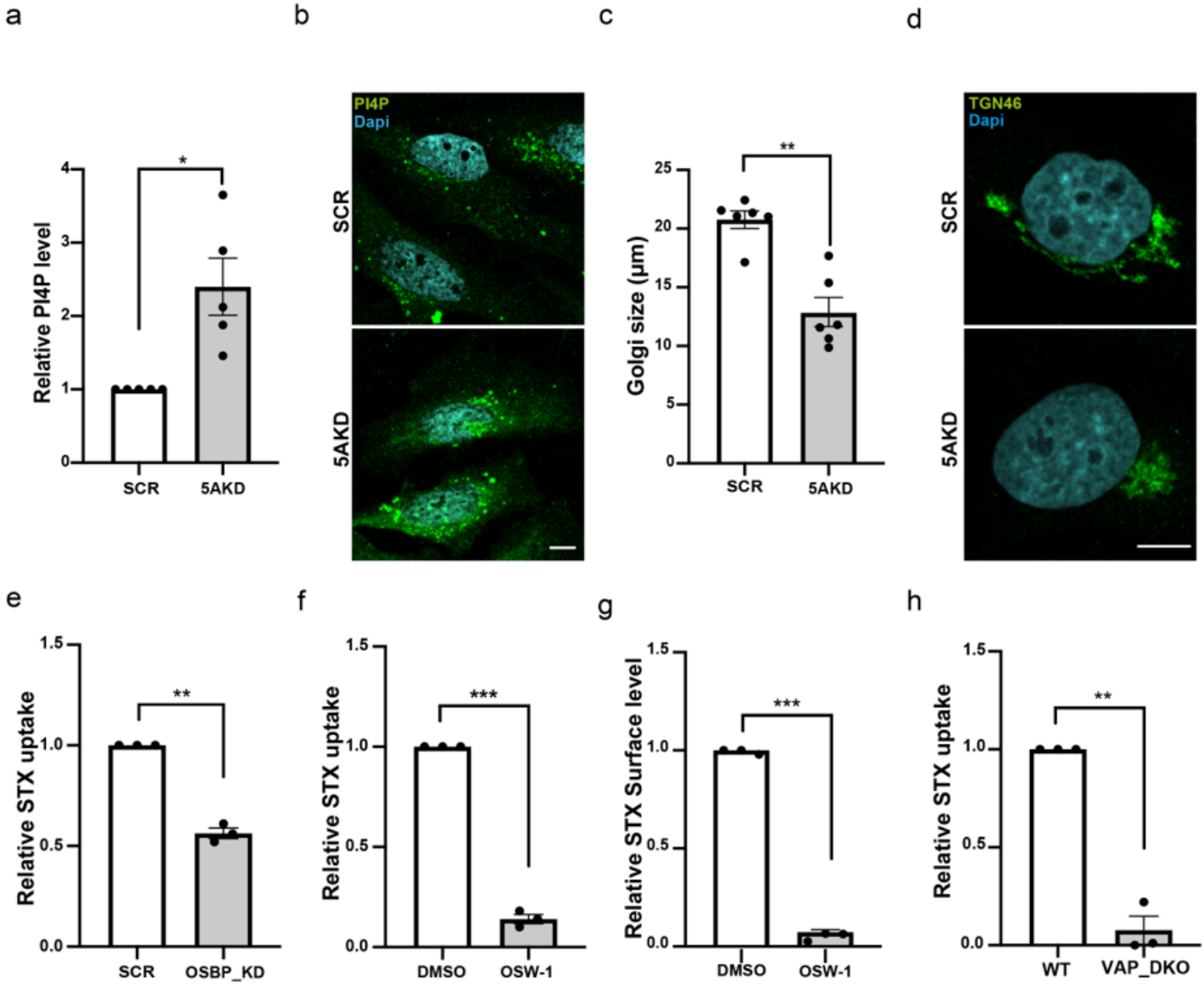

Figure 4

Impaired cholesterol/ PI(4)P lipid exchange at ER/ Golgi membrane contact sites blocks glycosphingolipid-dependent CIE of Shiga toxin (a) Relative phosphatidylinositol 4-phosphate [PI(4)P] levels in HeLa cells treated with control (SCR, set to 1) or INPP5A siRNA (5AKD). p = 0.0229, t = 3.594, df = 4. (b) Representative confocal images of HeLa cells treated with control (SCR) or INPP5A siRNA (5AKD) and stained for PI(4)P (green). Blue, DAPI-stained nuclei. Scale Bar, 10 µm. (c) Size of trans-Golgi network marked by TGN46 in HeLa cells treated with control (SCR, set to 1) or INPP5A siRNA (5AKD). Data are expressed in micrometer (length of long axis) . Two-tailed paired student's t-test p = 0.0013 , t = 6.474, df =5. (d) Representative confocal images of HeLa cells treated with control (SCR) or INPP5A siRNA (5AKD) and stained for the trans-Golgi marker TGN46 (green). Blue, DAPI-stained nuclei. Scale bar , 10 µm. (e) Relative STX uptake into HeLa cells treated with either control siRNA (SCR, set to 1) or siRNA against OSBP (OSBP_KD). One sample student's t-test: p = 0.0035, t = 16.77, df = 2. (f,g) Relative STX uptake (g) STX surface level (h) into HeLa cells treated with either DMSO (set to 1) or the specific OSBP inhibitor OSW-1 (20 nM, 16h). One sample student's t-test Uptake : p = 0.0007 , t = 37.24, df = 2. Surface: p =0.0002, t =71.32, df =2. (h) Relative STX uptake into wild-type or VAP-A/B double knockout (VAP DKO) HeLa cells. Data for wild-type HeLa cells were set to 1. One sample student's t-test: p = 0.006, t = 12.87, df = 2.

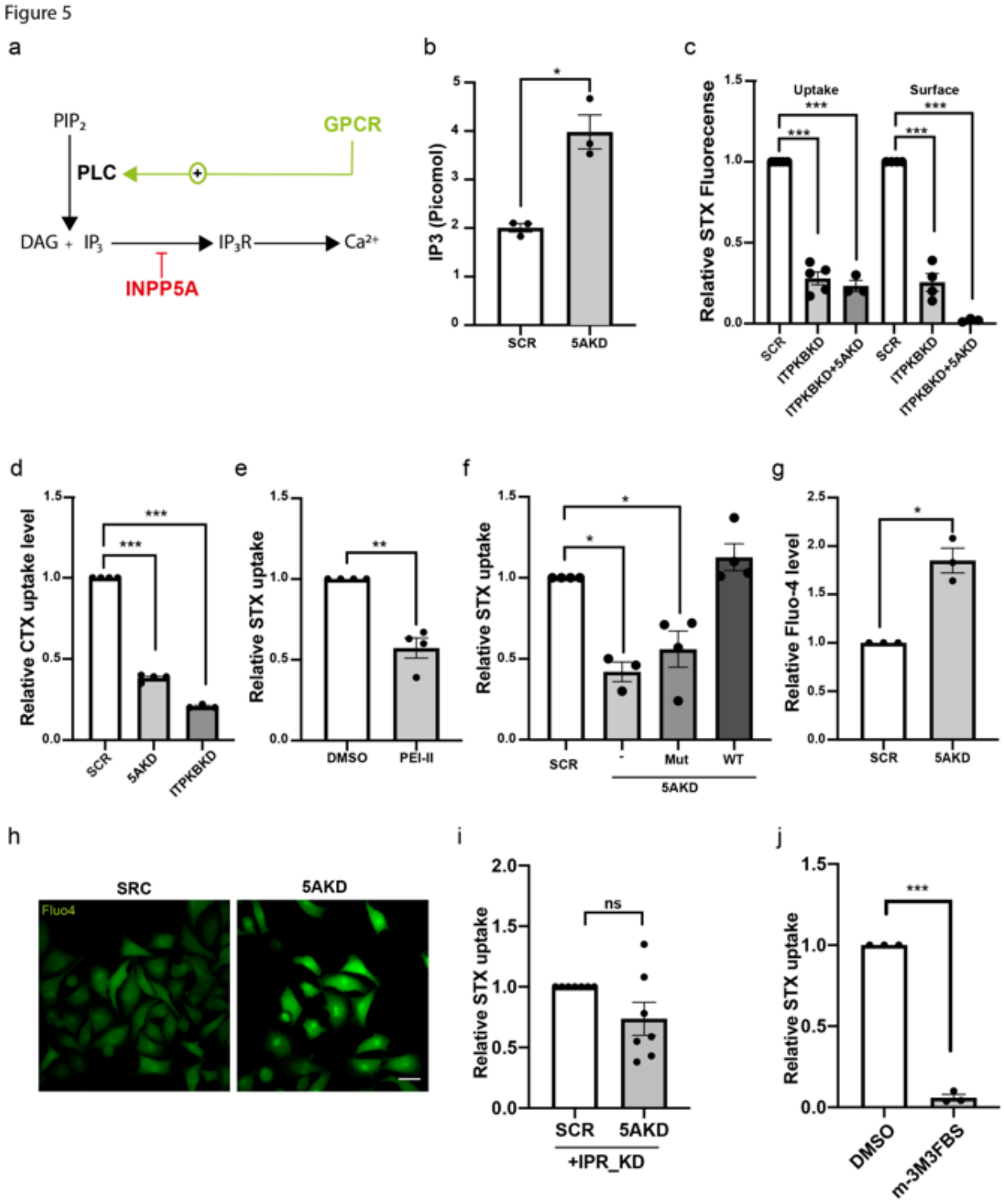

Figure 5

INPP5A controls surface glycosphingolipid homeostasis by regulating inositol 1,4,5-triphosphate levels. (a) Schematic representation of phospholipase C (PLC)-mediated cleavage of phosphatidylinositol 4,5-bisphosphate (PIP2) into diacylglycerol (DAG) and IP3 downstream of receptor (e.g. via G protein-coupled receptors, GPCRs) signaling. IP3 triggers Ca2+ release from the ER via IP3 receptors (IP3R), a pathway repressed by INPP5A-mediated IP3 hydrolysis. (b) Intracellular levels of inositol 1,4,5-triphosphate [IP3] in

HeLa cells treated with control or INPP5A siRNA (5AKD). Data expressed in pico mol / 500.000 cells. Two-tailed paired student's t-test, p = 0.0265 , t = 6.021, df = 2. (c) Relative Shiga toxin (STX; 5 µg/ml) surface binding (Surface) and endocytosis (Uptake) in HeLa cells treated with the indicated smart pool siRNAs. Data for SCR-control siRNA-treated cells for Uptake or Surface labaling assays were set to 1. (ITPKB, inositol triphosphosphate kinase B). One sample student's t-test followed by Benjamini Hochberg correction. Uptake ITPKBKD : p = 0.0002 , t = 18.47 , df = 4 . Uptake ITPKBKD+5AKD : p = 0.0019 , t = 23 , df = 2 . Surface ITPKBKD : p = 0.0002 , t = 13.66 , df =3. Surface ITPKBKD+5AKD : p = 0.0008 , t = 169.7 , df =2. (d) Relative Cholera toxin (CTX; 5 µg/ml) uptake in HeLa cells treated with the indicated siRNAs. Data for SCR-control siRNA-treated cells were set to 1. One sample student's t-test followed by Benjamini Hochberg correction. 5AKD: p <0.0001, t =55.7, df =3. ITPKB: p<0.0001, t =119.0, df =2. (e) Relative Shiga toxin (STX; 5 µg/ml) endocytosis in HeLa cells treated with DMSO or the prolyl endopeptidase inhibitor 2 PEI-II known to result in increased IP(1,4,5)P3 levels. One sample student's t-test : p = 0.0064 , t = 6.84 , df =3. (f) Defective STX endocytosis is rescued by re-expression of siRNA-resistant active wild-type (WT) but not phosphatase-defective inactive mutant (Mut) INPP5A. Data for SCR-control siRNA-treated cells were set to 1. One sample student's t-test followed by Benjamini Hochberg correction . -/5AKD: p = 0.0327 , t = 9.492 , df =2 . Mut/5AKD: p = 0.0.0435 , t = 3.456 , df =2 . Res/5AKD : p = 0.2225 , t = 1.534 , df =3 . (g,h) Loss of INPP5A results in elevated intracellular calcium levels. Representative confocal images (h) and quantified Fluo-4 staining (g) of HeLa cells treated with control (SCR, set to 1) or INPP5A siRNA (5AKD). Scale bar, 25 µm. One sample student's t-test . 5AKD: p = 0.0217 , t =6.671 , df =.2 (i) Depletion of IP3-receptors rescues defective STX-endocytosis induced by loss of INPP5A. Relative Shiga toxin (STX; 5 µg/ml) endocytosis in HeLa cells treated with the indicated smart pool siRNAs. Data for SCR-control siRNA combined to IPRs siRNA treated cells were set to 1. One sample student's t-test 5AKD+IPRs_KD : p =0.1009 , t = 1.937 , df =6 . (j) Pharmacological activation of PLC by m-3M3FBS inhibits CIE of Shiga toxin in HeLa cells. Data for DMSO-treated control cells were set to 1. One sample student's t-test 5AKD+IPRs_KD : p =0.0005 , t = 46.51 , df =2. Numerical source data and unprocessed blots are reported in the Source Data f

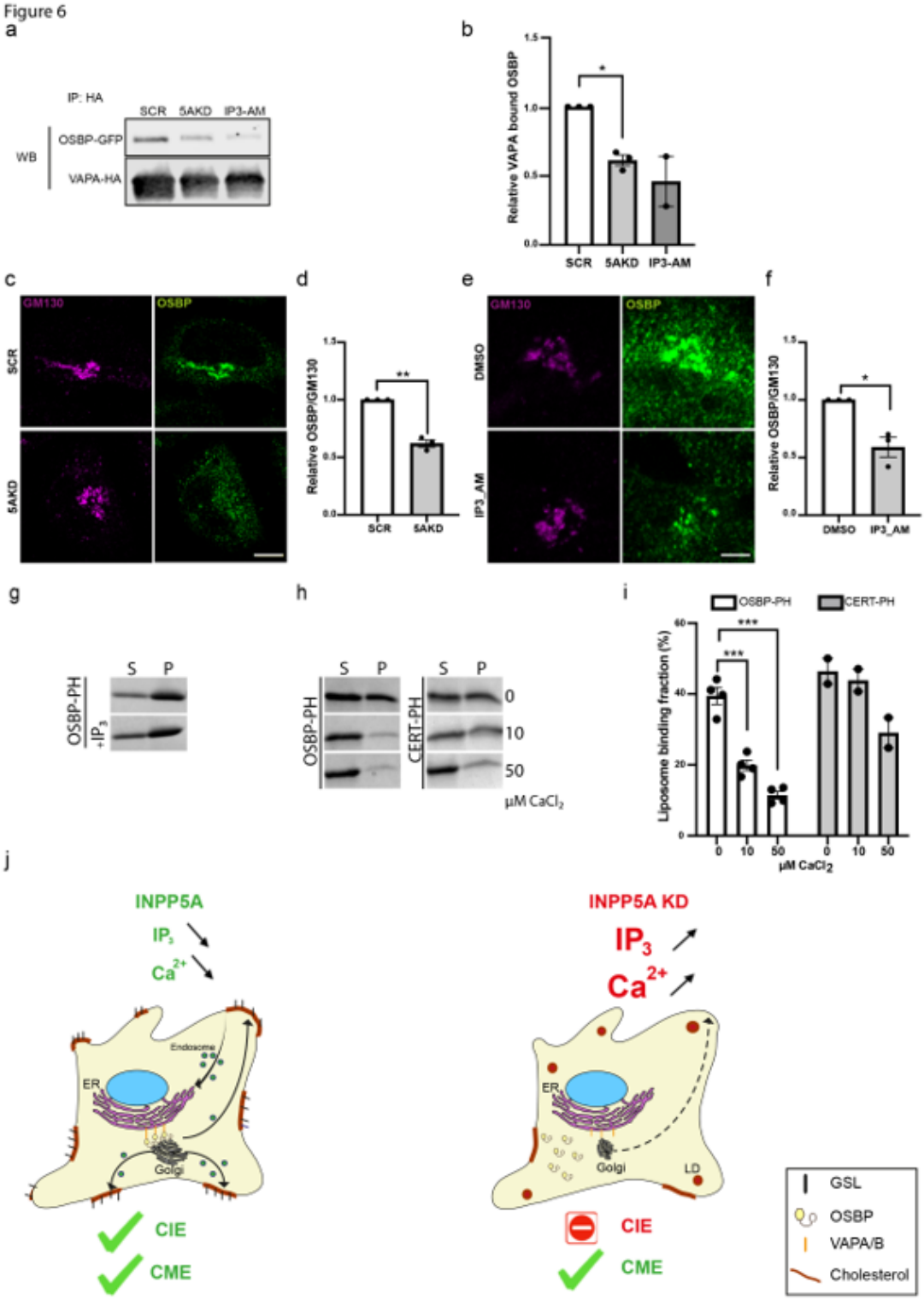

Figure 6

IP3-mediated calcium release represses lipid exchange at ER/ Golgi contact sites by inhibiting OSBP recruitment and function. (a) HEK-293T cells treated with either control siRNA (SCR) or siRNA against INPP5A (5AKD) or SCR-siRNA plus 50□□M of IP3/ AM (2h) and co-expressing VAP-A-HA and OSBP-GFP were lysed and subjected to immunoprecipitation with anti-HA antibodies covalently linked to magnetic beads. Samples were analyzed by immunoblotting for the HA epitope tag or GFP. Representative data are

shown. (b) Quantification of representative data shown in (a). The amount of OSBP-GFP co-precipitated with VAP-A-HA under SCR-control conditions was set to 1. Data represent mean ± SEM from n=3 independent experiments for 5AKD and n=2 for I IP3/AM. One sample student's t-test 5AKD: p = 0.0097, t = 10.06 , df = 2. (c,e) Representative confocal images (c) of HeLa cells treated with either control siRNA (SCR) or siRNA against INPP5A (5AKD) (e) of HeLa cells treated with DMSO or 50μM of IP3_AM. stained for endogenous GM130 as a Golgi marker (Magenta) and OSBP (green). DAPI-stained nuclei are shown in blue. Scale bar 10 μm . (d,f) shows the relative levels of endogenous OSBP localized to the Golgi complex marked by GM130. (d) in HeLa cells treated with negative control SCR or siRNA for INPP5A. (f) in HeLa cells treated with DMSO or 50 M of IP3_AM. control cells were set to 1. one sample student's t-test. 5AKD: p = 0.0071, t = 11.82, df = 2. IP3_AM p = 0.00415, t = 2.755, df = 2. (g-i) Liposome co-sedimentation assays to determine binding of purified recombinant OSBP-PH or CERT-PH to PI(4)P-containing liposomes. S, supernatant; P, liposomal pellet. Samples were analyzed by SDS-PAGE and staining with Coomassie Blue. Representative data for IP3 effect are shown in (g) and for Calcium effect in (h). Quantification of representative PI(4)P-liposome binding assays shown in (i). Orinary one way ANOVA using Dunett's multiple comparaison test. (0 vs 10 μM): p<0.0001. (0 vs50 μM): p = <0.0001. Data represent mean ± SEM from at n=3 independent experiments for OSBP-PH domain and n=2 for CERT-PH domain. Numerical source data and unprocessed blots are reported in the Source Data file. (h) Hypothetical model for the role of INPP5A-mediated turnover of IP3 in the regulation of cholesterol export at ER-Golgi membrane contact sites and its sconsequences for cell physiology. Numerical source data and unprocessed blots are reported in the Source Data file.